




# Monitoring the Grassland Change in the Qinghai-Tibetan Plateau: A Case Study on Aba County

Qiufang Shao<sup>1</sup> · Yue Shi<sup>1</sup> · Zhiying Xiang<sup>2</sup> · Huaiyong Shao<sup>1,3,4</sup>  · Wei Xian<sup>5</sup> · Peihao Peng<sup>3</sup> · Chengying Li<sup>1</sup> · Qiorong Li<sup>1</sup>

Received: 11 February 2017 / Accepted: 9 October 2017 / Published online: 1 December 2017  
© Indian Society of Remote Sensing 2017

## Abstract

Located on the southeast edge of the Qinghai-Tibetan plateau, Aba County is the core area of the Returning Grazing Land to Grassland Project (RGLGP) on the plateau. For the purpose of monitoring the grassland change before and after the grassland protection project in Aba County, Landsat images acquired in 1996, 2003 and 2009 were analyzed. Using Spectral Mixture Analysis (SMA) model, sub-pixel fractions of land cover components were obtained: bright vegetation (BV), dark vegetation (DV), bright soil (BS), dark soil (DS) and water. Fraction images present the distribution and proportions of typical land cover components in this study. Fractions BV and BS were chosen as two indicators for grassland degradation. Thereafter, Change Vector Analysis (CVA) model was applied on the two indicators. After the performance of the CVA model, change results which consisted of both grassland degradation and vegetation re-growth were obtained, showing the change patterns of grassland degradation and vegetation re-growing in Aba County between two gaps: from 1996 to 2003 (before the RGLGP) and from 2003 to 2009 (after the RGLGP). The change patterns of grassland degradation and vegetation re-growing can effectively assist in the development of environmental restoration measures and in the RGLGP plans for the Qinghai-Tibetan plateau.

**Keywords** Aba County · Spectral mixture analysis · The grassland change · The Qinghai-Tibetan plateau · The returning grazing land to grassland project

## Introduction

China is one of the few countries in the world that possess a wide grassland area (Li et al. 2015). Grassland ecosystem plays a crucial role in biodiversity, water and soil

conservation, climate regulation, husbandry development and ecological balance (Shao et al. 2016). Nevertheless, since the 1950s, the long, unscientific land use trends in China's grassland areas have given rise to environmental problems such as livestock over-grazing and artificial excess reclamation (Fan et al. 2007). As the grassland eco-environment continues to worsen, the Chinese government has successively carried out the Return Grazing Land to Grassland Project (RGLGP) (Ministry of Agriculture 2014). Monitoring grassland change before and after the RGLGP not only can provide scientific evidences for further planning grassland protection strategies, but also presents as a crucial academic task for researchers (Li et al. 2011; Zhang et al. 2014; Shao et al. 2016). At this moment, remote sensing techniques, which are ideal for measurement of local, regional and global surface radiation (Geerken and Ilaiwi 2004; Mukherjee et al. 2009), stand out as a time- and cost- effective method for monitoring grassland change (Wessels et al. 2008; Beyene 2013).

---

✉ Huaiyong Shao  
huaiyongshao@163.com

<sup>1</sup> College of Earth Science, Chengdu University of Technology, Chengdu, Sichuan, China  
<sup>2</sup> School of Earth Sciences, Zhejiang University, Hangzhou, Zhejiang, China  
<sup>3</sup> Key Laboratory of Geoscience Spatial Information Technology of Ministry of Land and Resources, Chengdu University of Technology, Chengdu, Sichuan, China  
<sup>4</sup> Center for Global Change and Earth Observations, Michigan State University, East Lansing, MI, USA  
<sup>5</sup> College of Resources and Environment, Chengdu University of Information Technology, Chengdu, Sichuan, China

Traditionally, researchers have focused on detecting grassland degradation changes affected by grassland eco-environment restoration projects in north China, under dry semiarid ecosystems. They have conducted detection approaches, established degradation indicator systems, and pointed out the spatial–temporal change pattern and the driving forces of grassland degradation conditions in north China (Huang and Siegert 2006). In recent years, the focus has been turned to the grassland degradation in west China, especially in the Qinghai-Tibetan plateau, which contains high biodiversity and enjoys fragile alpine- and sub-alpine environments (Harris 2009; Li et al. 2013a, b; Dong et al. 2015). However, the grassland change in the Qinghai-Tibetan plateau before and after the RGLGP still lacks research.

In the remote sensing images of the Qinghai-Tibetan plateau where grassland, wetland, shrub and sandy soils are distributed closely, one pixel usually contains mixed spectral information due to the high variability in the distribution of land cover components. Commonly applied approaches to detecting grassland change are pixel-level sensitive vegetation indices. For example, NDVI, can be negatively influenced by soil background, especially for bright soils and sparse vegetation canopies (Röder et al. 2008; Chien et al. 2016). Hence, a multi-endmember Spectral Mixture Analysis (SMA) model is designed to derive the proportions of vegetation, sandy soil and water that compose a mixed pixel to monitor grassland change in a precise way. SMA has been proven effective in a variety of quantitative applications with multispectral imagery ranging from arid-/semi-arid environment (Collado et al. 2002; Dennison and Roberts 2003; Dawelbait and Morari 2012), moist tropical environment (Lu et al. 2004) to urban environment (Peddle et al. 1999; Small 2001; Okin and Roberts 2004; Powell et al. 2007). Nevertheless, applying SMA to monitor grassland change in the grassland environment is an innovative attempt. Moreover, As SMA derived several sub-pixel land cover fractions, bright soil fraction and bright vegetation fraction were selected out to conduct Change Vector Analysis (CVA) to acquire vegetation cover change pattern in this region. Specifically, CVA results assisted us to distinguish degradation and vegetation-regrowth by calculating difference between corresponding pixels for each fraction.

In sum, this paper chose a fragile region on the southeast edge of the Qinghai-Tibetan plateau as the study area, Aba County, where RGLGP has been practiced since 2003. Using satellite images from 1996 (before the RGLGP), 2003 (when the RGLGP started), and 2009 (after the RGLGP), this paper conducted a grassland change monitoring study by applying SMA and CVA. Through our study, spatial–temporal change of the grassland in Aba County was obtained, which revealed that the grassland

change was influenced by the RGLGP. Moreover, our study results also can assist on further designing the strategy of the RGLGP in a scientific way.

## Study Area

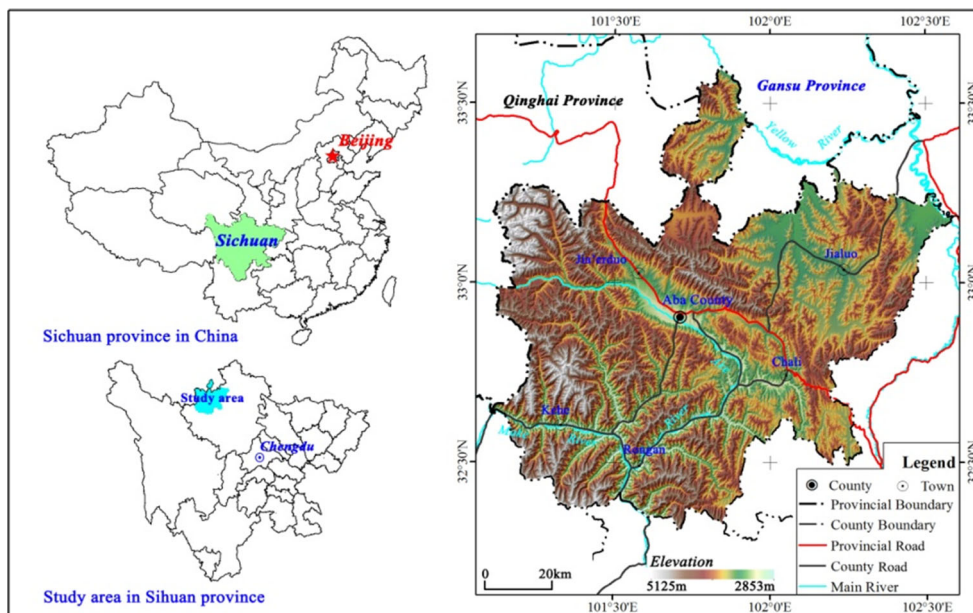
Aba County (Fig. 1), which is one of the priority protection counties in the river-source region of the Qinghai-Tibetan plateau for its critical geographic position and significant water conservation function, was chosen as our case study area for its core position in the RGLGP. Aba County, covering approximately 10,435 km<sup>2</sup>, is located on the southeast edge of the Qinghai-Tibet Plateau (between latitude 32°18' to 33°37'N and longitude 101°18' to 102°35'E), where the headwaters of the Yellow River flow. The plateau's hills and alpine valleys form its landscape with an altitude ranging from 3479 to 3764 m. An annual average rainfall close to 712 mm is received each year. The climate in Aba County is a typical sub-humid plateau in a frigid temperate zone with an annual average temperature around 3.3 °C. Subalpine grasslands, which are consisted of grassland, wetland and shrub, are distributed widely across Aba County, accounting for 85.1% of its total land area (Aba County People's Government 2012). Therefore, pastoral farming has been a major part of local husbandry for centuries. In Aba grasslands, dominate vegetation types (certain types of vegetation which has a large area in the study area) are subalpine meadow, alpine meadow and marsh-meadow; and dominate soil types are peat moor soil, alpine meadow soil, sub-alpine meadow soil and swampy meadow soil. Due to its unique geographic position and crucial water conservation function, Aba County plays a crucial role as part of the ecological barrier for southwest China.

## Materials and Methods

### Data Acquisition and Preprocessing

Downloaded from Geospatial Data Cloud (<http://www.gscloud.cn/>, supported by CAS data center), six scenes from the Landsat-5 Thematic Mapper (TM) from 1996, 2003 and 2009 (orbit numbers 131/37, 131/38) with high data quality and low cloud cover percentage were selected. All six scenes were recorded between August and September when vegetation grew well because degraded grasslands are more easily recognized during this period. Grassland degradation refers to the decline of grassland vegetation coverage and quality, deterioration of soil habitat, decline in productivity and ecological function due to causes such as overgrazing, burrowing of small mammals, and climate change (Akiyama and Kawamura 2007).

**Fig. 1** Geographic location of Aba County



To apply the SMA model, the six images for the study area were atmospherically calibrated and then converted from digital number (DN) into at-satellite reflectance. Landsat-5 TM has a spatial resolution of 30 m with six visible/near infrared bands and one thermal band. Band 6 (10.4–12.5 μm) is not included in the analysis because the thermal infrared wavelengths are not required for performing atmospheric calibration. The conversion process to transform reflectance spectra of materials from reflectance into relative radiance first requires a conversion of the DN to quantitative physical values such reflectance radiance. For each of the six bands, the at-satellite radiances  $L$  were calculated using the equation:

$$L = \frac{L_{max} - L_{min}}{QCAL_{max} - QCAL_{min}} * (QCAL - QCAL_{min}) + L_{min} \tag{1}$$

where  $L$  is the spectral radiance at the sensor aperture in watts,  $QCAL$  refers to the quantized calibrated pixel value in DN,  $QCAL_{min}$  refers to the minimum quantized calibrated pixel value,  $QCAL_{max}$  refers to the maximum quantized calibrated pixel value,  $L_{min}$  refers to the spectral radiance that is scaled to  $QCAL_{min}$ ,  $L_{max}$  refers to the spectral radiance that is quantized to  $QCAL_{max}$ . At-satellite reflectance is given by the following equation for each of the six bands:

$$\rho_i = \frac{\pi * L * D^2}{ESUN * COS\theta} \tag{2}$$

where  $\rho_i$  is the unit at-satellite reflectance of band  $i$ ,  $D$  is the earth-sun distance in astronomical units,  $ESUN$  is the mean solar atmosphere irradiances (band specific) in W m μm,  $\theta$  is the solar zenith angle in degrees,  $L$  is the spectral radiance in W m μm. Each TM image is geo-registered to

the rectified Landsat-5 TM 2007 image using nearest neighbor re-sampling with 36 control points, an average RMS error of 0.5 is calculated, which is appropriate for multi-temporal comparisons.

### Spectral Mixture Analysis (SMA)

SMA models derive each pixel-reflectance into the fractions of representative surface materials (endmembers) using high spectral resolution reflectance measurements collected from airborne or space borne spectrometers (Asner et al. 2003). One basic assumption of SMA model is that the spectrum for each pixel is a linear or nonlinear combination of endmember spectra dependent on the significance of multiple light scattering on land cover types (Wu 2004). Furthermore, linear SMA models, which assume that the spectral reflectance profile of each pixel is a linear combination of typical endmembers, are classically utilized and proven to be effective (Wu and Murray 2003). In order to explain the mixed reflectance signal of each pixel in a grassland environment, a fully constrained linear SMA method was applied by using the appropriate end-member spectra obtained from TM images:

$$R_j = \sum_{i=1}^N f_i R_{i,j} + e_j \tag{3}$$

$$\sum_{i=1}^N f_i = 1 \quad \text{and} \quad f_i \geq 0 \tag{4}$$

$$RMS = \sqrt{\sum_{j=1}^M \frac{(e_j)^2}{M}} \tag{5}$$

where  $R_b$  is the reflectance for each band  $k$  in a pixel,  $f_i$  is the fractional abundance of endmember  $i$ ,  $R_{i,j}$  is the reflectance of endmember  $i$  in band  $j$  for that pixel,  $N$  is the number of spectral endmembers,  $R_j$  is the residual, and  $M$  is the total number of spectral bands. Associated with determining  $R_j$ ,  $\sum_{i=1}^N f_i = 1$  and  $f_i \geq 0$  were required. For this analysis with TM data, there will be six equations, one for each spectral band ( $M = 6$ ). Equation (5) is the total root-mean square (RMS) error to assess model fitness.

### Endmember Selection

As shown in the Eqs. (3)–(5), the validity of the SMA model depends on the selection of endmembers. Previously, Elmore et al. (2000) stated that endmembers must define a coherent set of spectra that are representative of physical components on the surface. Endmembers can be identified using either laboratory-based measurements of endmember's spectra (Wu and Murray 2003), referred to as "reference endmember", or spectrally pure or "extreme" pixels identified within the images being analyzed (Myint and Okin 2009), which referred to as "image endmember". Although image endmembers cannot be entirely pure, their degree of pureness is more accurate as they represent the dimensionality of the corresponding data set. In this study of monitoring grassland change, image endmembers were chosen and derived from the Landsat-5 TM images.

In this study, endmembers from the three dates of the Landsat-5 TM images were derived with the following steps: first, a spectral reduction procedure was performed by the Minimum Noise Fraction (MNF) transform; second, spatial reduction procedure was performed by the Pixel Purity Index (PPI) method; and third, manual identification of the endmembers was performed using the N-dimensional visualizer. In the first step, the MNF transform, which consists of two consecutive data reduction operations, aims to ensure valid dimensions of reflectance data by separating noise from it, thereby reducing the amount of calculation in later procedures (Green et al. 1988). After that, the PPI, which has been widely used in multispectral and hyper-spectral image analysis for endmember extraction, aims to search for a set of vertices of a convex geometry in a given data set that are supposed to represent pure signatures present in the data (Chaudhry et al. 2006). Finally, by adding in PPI results (relatively pure pixels), an interactive tool N-dimensional visualizer is utilized, which can interactively assist researchers to identify image endmembers in N-dimensional space. For each date of reflectance data, five endmembers were identified according to the feature spaces and their associated interpretations obtained from the original reflectance data. These endmembers are: bright vegetation, e.g. meadow, marsh-

meadow and shrubs (BV); dark vegetation, e.g. senescing meadow and senescing shrubs (DV); bright soil, referring to sandy soil with high reflectance and low water content (BS); dark soil, referring to bare soils with low reflectance and high water content (DS); and water. All the end-member spectra of 1996, 2003, and 2009 are shown in Fig. 2.

### Fraction Image Calculation

As stated by Brandt and Townsend (2006), using identical image endmembers for multi-temporal images allows a direct comparison of resulting endmember proportions. In this study, proportions of BV, DV, BS, DS and water for each TM image, presented as fraction images, were calculated by solving a fully constrained five-endmember linear SMA model using the Landsat TM imagery data. The mean RMS error for each image ranges from 0.005 to 0.008, which suggests a generally good fit (less than 0.02). Calculated fraction images represent the quantitative proportions as well as the general distribution of vegetation cover and soil cover in 1996, 2003 and 2009. Visually, by comparing multi-temporal BS fraction images of a sample patch in northeast Aba grasslands (Fig. 3), a tendency of soil cover expansion is presented, which indicates the grassland change in this area. By comparing multi-temporal BV fraction images of another sample patch nearby (Fig. 4), a tendency of vegetation cover reduction is presented, which also indicates the grassland change in this area. In detail, fraction images are results of sub-pixel classification; thereby, they contain precise proportions of surface components in Aba grasslands, which will contribute to change the detection model for grassland change in this study.

### Change Vector Analysis (CVA) Model

CVA model examines the corresponding pixels of two satellite images by comparing two bands of each image to produce images of change magnitude and change direction (Kuzera et al. 2005). In this paper, BV and BS fraction images were used to monitor the grassland degradation and vegetation re-growing at Aba County between two gaps: from 1996 to 2003 and from 2003 to 2009. The change magnitude of the vector is calculated from the Euclidean Distance. The results show the difference between the pixel values of the fraction images for BV and BS cover respectively. It is shown as follows:

$$R = \sqrt{(BS_1 - BS_2)^2 + (BV_1 - BV_2)^2} \quad (6)$$

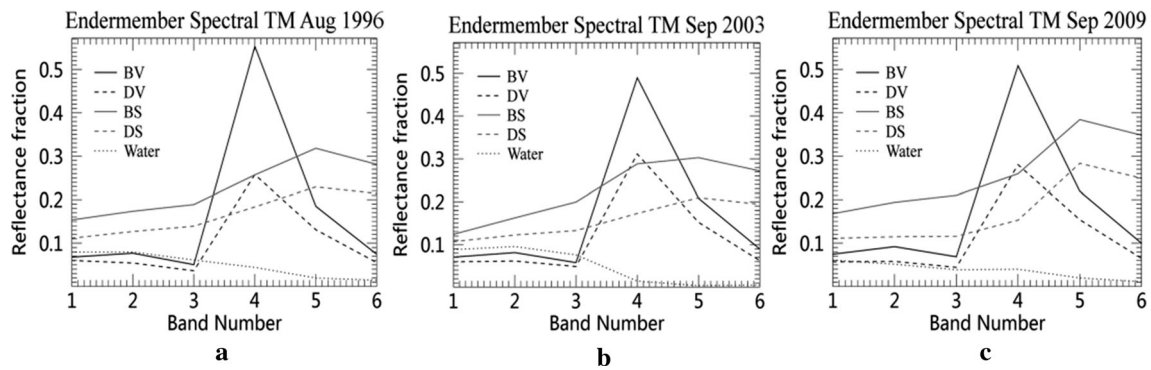


**Fig. 2** Endmember Spectra in 1996, 2003 and 2009 (left to right as a, b, c in the above) where BV represents bright vegetation component, DV represents dark vegetation component, BS represents bright soil component, and DS represents dark soil component

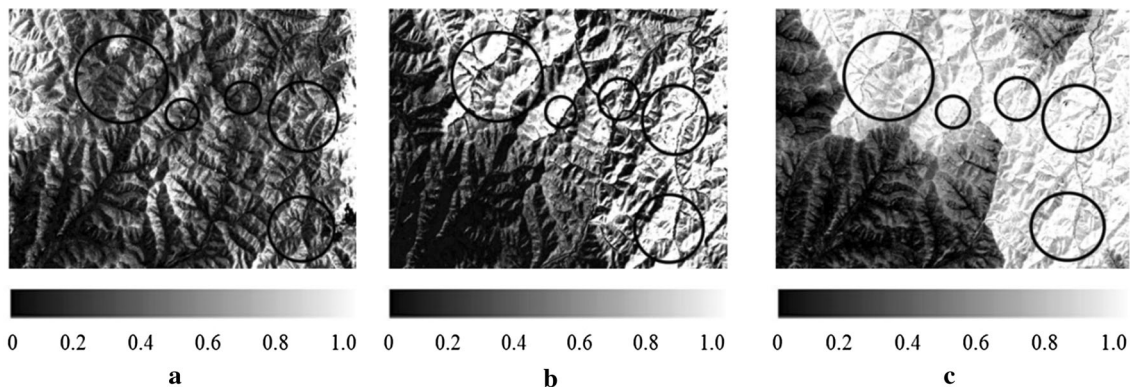


**Fig. 3** Change tendency of BS fraction images: **a** BS in 1996; **b** BS in 2003; and **c** BS in 2009

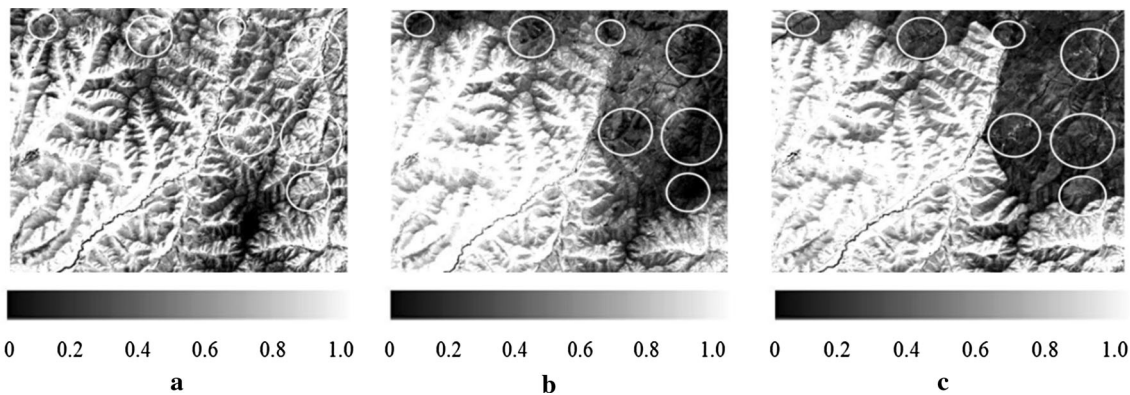


**Fig. 4** Change tendency of BV fraction images: **a** BV in 1996; **b** BV in 2003; and **c** BV in 2009

where  $R$  is the magnitude of vector change, and subscript 1 and 2 indicate the fraction covers in early date and later date.

Change direction is measured as the angle ( $\alpha$ ) of the change vector from a pixel measurement in early date to the corresponding pixel in later date according to:

$$\tan \alpha = (BS_1 - BS_2) / (BV_1 - BV_2) \tag{7}$$

Angles measured between  $90^\circ$  and  $180^\circ$  indicated an increase in sandy soil and decrease in vegetation cover and therefore represent grassland change conditions. Meanwhile, angles measured between  $270^\circ$  and  $360^\circ$  indicate a decrease in sandy soil and an increase in vegetation cover and therefore represent vegetation re-growing conditions (Lorena et al. 2002). Angles measured between  $0^\circ$ – $90^\circ$  and  $180^\circ$ – $270^\circ$  indicate either an increase or decrease in both

sandy soil and vegetation cover, and consequently persistent conditions.

### Gradation of the Grassland Change

The resulting value of the grassland change obtained from SMA is continuous. A classification of the different levels of the grassland change should be made so as to acquire an overall understanding of the regional grassland change (Shao et al. 2014). Natural breaks classification is a data classification method designed to determine the best arrangement of values into different categories. This is done by seeking to minimize each class's average deviation from the mean of the category, while maximize each class's deviation from the means of the other groups (Jenks 1967; McMaster and McMaster 2002; Shao et al. 2014). Natural breaks classification is a "natural" classification method, which meet "birds of a feather flock together". The difference is obvious between different categories, while very small inside a category, and there is a more obvious break between category and category. Therefore, natural breaks classification is used to analyze the natural properties of the grassland change results to find out the breakpoints (thresholds) and thus divide the grassland change into different levels in study area. According to existing research results (Chen et al. 2013; Li et al. 2013a, b; Shao et al. 2014; Zhang 2006), Grassland Degradation and Vegetation Re-growing in our study area are divided into three levels: low, medium, high. As shown in Table 1, each level of Grassland Degradation has its own typical characteristics (Li and Du 2013; Ren 1998).

### Data accuracy Verification Through Field Investigation

In order to evaluate the accuracy of SMA, a field survey was conducted in August 2009 using ground vegetation data as a reference. A total of 20 sampling sites (size  $60 \times 60$  m for each site, corresponding to 4 pixels of Landsat image) were located and established in the study area. At each site, trees and bushes were geo-referenced with a GPS, the percentage of ground vegetation cover including subalpine meadow was taken, and marsh-meadow and shrubs were estimated using the line-point intercept sampling method. Measurements were taken along 20 60-m-long transects oriented in N-S direction. Pin flags were lowered at 2 m intervals along the entire length of transect. At each point, the types of cover were recorded and the percentage of vegetation cover was calculated. The accuracy of SMA was estimated by scatter plotting correlations of the total percentage of vegetation cover in each plot and the vegetation fraction image (Fig. 5).  $R^2$  of 0.811 represents an appropriate correlation between them. There are possible resources of error that may have affected the correlation result, including geometric rectification error, survey sampling error and cloud shadow of images.

In order to verify the accuracy of the classified map, we conducted field survey regarding grassland change conditions along with interviewing local pastoralists on historical change status. As shown in Fig. 6, we established 180 field sampling points in total, with 30 points for each classified degradation or re-growing level. By comparing remote sensing monitoring results with field validation data, the general accuracy of grassland degradation level classification achieved 92.56%, which contributed to reveal

**Table 1** Results of the grassland degradation classification in the Qinghai-Tibetan plateau

Levels of grassland degradation	Character description
Low	Grassland community basically maintains primary dominant species, while high quality forage slightly decreases both in coverage and productivity. Meanwhile, among grassland community, species with strong adaptability and poor palatability gradually increases in amount. In addition, minor degradation detected in sampling plots indicates invasion of poisonous or harmful plants
Medium	Plant species and appearance changes obviously. Specifically, primary dominant species degrade causing the decrease of high quality in amount and therefore affects both coverage and productivity negatively. Moreover, the proportion of forbs with strong adaptability and poor palatability continues increasing so as poisonous and harmful plants. The sampling plots suffers from the rise of degradation indicator plants and uneatable forbs, along with the apparent existence of saline-alkaline patches erosion and mouse holes
High	Dominant plants in grassland community changes significantly from its primary stage, especially in some worsen areas where native grass species have been replaced partially or completely. In this level, dominant species or communities in grassland are replaced by forbs with strong adaptability and poor palatability or poisonous and harmful plants. With the booming of degradation indicator plants, eatable forage drops down badly. Bare land patches sprawl through grassland, while mouse holes increase obviously. Grassland surface suffers from overwhelming wind erosion, water erosion, freeze-thaw, salinization and desertification. In some areas, grassland community has been replaced by secondary community completely

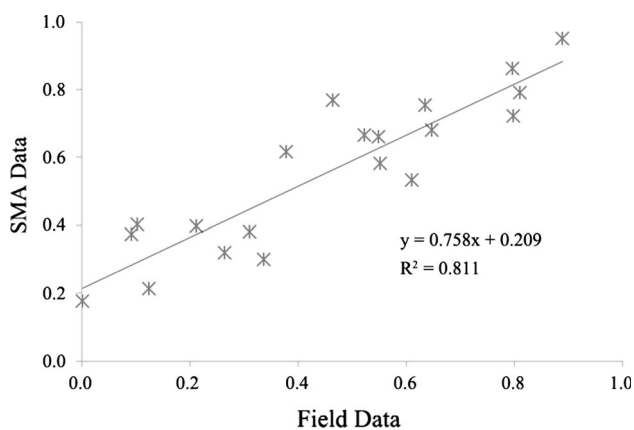


**Fig. 5** Scatter plot correlation between measured and SMA estimated vegetation fraction

change patterns of regional grassland degradation in a macroscopic and objective perspective.

## Results and Discussion

### Change Detection Results

CVA assists on the derivation of multi-temporal land cover change information, along with providing specific change vector magnitude and direction (Nackaerts et al. 2005). Though previously it has been mainly applied on forestry land cover change detection (The Animal Husbandry

Bureau of Sichuan Province 2012), CVA performed efficiently and accurately as well in our case study on grassland change. Adopting vegetation and soil spectra provided by SMA, CVA model was run in ERDAS Software environment accomplishing calculation functions on both change direction and magnitude for each pixel. Calculation output layers were then transferred to ArcGIS environment for further mapping purposes.

The change directions, which are derived from CVA, indicate both grassland degradation and vegetation re-growing. The magnitude ranges from low level to high level for both grassland degradation condition and vegetation re-growing condition between 1996 and 2003 (Table 1, Fig. 6) as well as between 2003 and 2009 (Table 2, Fig. 7).

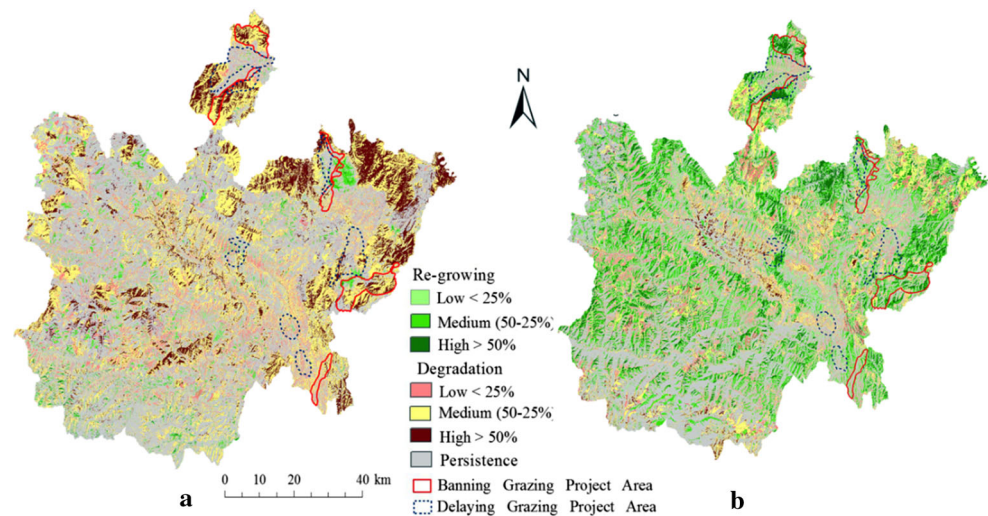
As shown in Table 2, the whole time period was divided as two parts. The first part was from 1996 to 2003 (before the RGLGP), when the degraded area covered 4861.62 km<sup>2</sup>, accounting for half of the study area. Medium level of degradation was significant, occupying 2825.08 km<sup>2</sup>; moreover, high level and low level degradation covered 1120.65 and 915.89 km<sup>2</sup>, respectively. In addition, the vegetation re-growing area covered 440.30 km<sup>2</sup> in total, accounting for 4.34% of the study area. Generally, during the period of 1996–2003, Aba County's rangeland degradation area prevailed against the vegetation re-growing area dramatically. The second time period was from 2003 to 2009 (after the RGLGP), when the vegetation re-growing area covered 3426.04 km<sup>2</sup>,

**Fig. 6** Photos of field validation on grassland change in the study area



**Table 2** Statistic table of grassland degradation and vegetation re-growing conditions in Aba County

Type	Level	From 1996 to 2003		From 2003 to 2009	
		km <sup>2</sup>	%	km <sup>2</sup>	%
Grassland degradation	Low	915.89	9.05	958.59	9.47
	Medium	2825.08	27.9	1243.59	12.28
	High	1120.65	11.07	145.04	1.43
	Total	4861.62	48.02	2347.22	23.18
Vegetation re-growing	Low	161.35	1.59	784.39	7.75
	Medium	257.52	2.54	1881.12	18.58
	High	21.43	0.21	760.53	7.51
	Total	440.30	4.34	3426.04	33.84
Persistence		4823.12	47.64	4351.78	42.98
Total		10,125.04	100	10,125.04	100

**Fig. 7** Distribution map of grassland degradation and vegetation re-growing areas between 1996 and 2003 (a) and between 2003 and 2009 (b) by applying change vector analysis model

accounting for 33.84% of the study area. Medium level of vegetation re-growing was significant, occupying 1881.12 km<sup>2</sup>; moreover, low level and high level of vegetation re-growing covered 784.39 and 760.53 km<sup>2</sup>, respectively. Meanwhile, degradation was also obvious, which occupied 2347.22 km<sup>2</sup> in total, accounting for 23.81% of study area. In detail, medium level degradation dominated the situation, covering 1243.59 km<sup>2</sup>, while low level and high level of degradation covered 958.59 and 145.04 km<sup>2</sup>, respectively.

Overall, between 1996 and 2003, grassland degradation prevailed over vegetation re-growing; between 2003 and 2009, vegetation re-growing prevailed over grassland degradation, while degradation still occupied a large amount of area.

### Rangeland Change Within and Outside of the RGLGP Area

In order to understand the rangeland change patterns before and after RGLGP, we counted the rangeland change within

RGLGP area (Table 3). As shown in Table 3, within project areas, severe rangeland degradation had existed before the RGLGP was carried out. That is, from 1996 to 2003, rangeland degradation covered 379.14 km<sup>2</sup>, accounting for 57.19% of the study area, while vegetation re-growing covered 26.01 km<sup>2</sup>, accounting for 3.92% of the study area. As for rangeland degradation, the medium level dominated the situation within the area of 223.21 km<sup>2</sup>, while high level and low level covered 97.08 and 58.85 km<sup>2</sup>, respectively. From 2003 to 2009, after the RGLGP was undertaken, proportions of rangeland degradation decreased while vegetation re-growing areas increased significantly. During this period, rangeland degradation occupied 129.66 km<sup>2</sup>, accounting for 19.55% of the study area, while vegetation re-growing occupied 268.29 km<sup>2</sup>, accounting for 40.46% of the study area. While rangeland degradation was dominated by medium level and low level across areas of 65.39 and 59.85 km<sup>2</sup>, respectively, vegetation re-growing was dominated by medium level with an area of 121.01 km<sup>2</sup>. Meanwhile, high level and low level covered 80.05 and 64.08 km<sup>2</sup>, respectively.



**Table 3** Statistic table of grassland degradation and vegetation re-growing within project areas

		From 1996 to 2003		From 2003 to 2009	
		km <sup>2</sup>	%	km <sup>2</sup>	%
Grassland degradation	Low	58.85	8.88	59.85	9.03
	Medium	223.21	33.67	65.39	9.86
	High	97.08	14.64	4.36	0.66
	Total	379.14	57.19	129.6	19.55
Vegetation re-growing	Low	9.86	1.49	64.08	9.67
	Medium	15.34	2.31	121.01	18.25
	High	0.81	0.12	80.05	12.07
	Total	26.01	3.92	265.14	39.99
Persistence		257.88	38.89	268.29	40.46
Total		663.03	100	663.03	100

### Comparison of SMA with Other Remote Sensing Monitoring Methods

At present, commonly applied remote sensing methods on grassland change monitoring include interactive visual interpretation method (Ghatol and Karale 2000; Krishan et al. 2009), supervised classification and unsupervised machine classification (Cai et al. 2014; Niu et al. 2013; Yang et al. 2014), vegetation indices (Cai et al. 2015; Liu et al. 2017), integrated indicators (Gao et al. 2010; Zhao et al. 2016). While visual interpretation method depends on expert knowledge and experience, it has limitations on both work efficiency and quantitative analysis regarding large amount of data bringing by multi-temporal grassland change. Machine classification methods such as supervised and unsupervised classification could achieve efficient change information extraction; however, the selection of its training samples is largely affected from artificial subjective factors. Moreover, grassland spectrum cluster generated from unsupervised classification method may not be suitable to identify grassland change types, and therefore raising the problem on matching actual grassland change conditions. Although vegetation indices are capable of accomplishing dynamic monitoring of grassland change efficiently using remote sensing products, the indices could just represent singular or limited characteristics of grassland degradation let alone revealing the comprehensive features of grassland change. Integrated indicator methods are likely to represent comprehensive features of grassland change, but how to reasonably assign its indicator weight is still a puzzling question.

In general terms, aforementioned remote sensing methods possess different advantages and short backs regarding grassland change monitoring. As to Qinghai-Tibetan Plateau, a single pixel usually contains multiple land cover types such as grassland, bare land, wetland et al. Above discussed methods extract grassland change information on

pixel level and therefore ignoring the fact that multiple types of land cover might appear in same pixel, which could possible affects monitoring results negatively. In this paper, a sub-pixel classification method, Spectral Mixture Model (SMA), was utilized to obtain spectrum of different land cover types in mixed pixels, identifying the proportions of major land cover types within a pixel. Using this method, Aba County was chosen as study area and its results are validated by field survey, which proves the efficiency and applicability of SMA on extracting land cover information in sub-alpine grassland environment. Aside of it, it should be mentioned that possible error sources could affect the precision of SMA model results, including the choice of GCP (ground control point) during geometric correction of images, clouds and shadows in images (might disturb endmember selection process), and uncertain manual error during field survey.

### Conclusions

Using multi-temporal remote sensing images, Spectral Mixture Analysis (SMA) provided us with sub-pixel classification results of land cover component of rangeland environment, avoiding possible misclassified area brought by traditional pixel-level category. Due to relatively simple structure of alpine rangeland landscape, we established spectra library containing five dominate components, among which BV and BS were highlighted for our study interest. Validated by field survey, those land cover information of interest with reliable accuracy was processed by Change Vector Analysis (CVA) which abstracted spectra information into high-dimension space to reveal land cover change patterns. Frankly speaking, CVA results assisted us to identify spatial-temporal distribution of grassland degradation and re-growing in rangeland environment.

Between 1996 and 2003, severe grassland degradation conditions in Aba County were concentrated in grassland areas where pastoral farming is the dominant practice. Since 2003, Aba and its neighboring territories have been returning the grazing land back to grassland. Thereby, vegetation re-growing conditions are detected in a wide range through Aba County between 2003 and 2009, but the rangeland degradation area still occupied a large portion. In accordance with study results, we can conclude the grassland in Aba County has a fragile eco-environment with a relevantly fast speed of degradation and a slow speed of reservation. Therefore, long-term grassland protection measures are still needed, in which large-scale remote sensing monitoring plays an indispensable role. Meanwhile, we suggest that it is consequential to continue quantitative research regarding the influence from climate change and human disturbance on rangeland degradation alongside conducting rangeland environmental resource capacity studies in order to assist the rangeland ecosystem protection and the further plans of the RGLGP in the Qinghai-Tibetan Plateau.

**Acknowledgements** This study is supported and funded by the National Natural Science Fund of China (Grant No. 41401659; Grant No. 41302282), the Science and Technology Department of Sichuan Province (Grant No. 2017SZ0088; Grant No. 2015JY0145), the Educational Commission of Sichuan Province (Grant No.13ZA0059; Grant No. 13ZB0089), Geological Survey Projects of Ministry of Land and Resources (Grant No. 1212011120019), and the National Undergraduate Training Programs for Innovation (Grant No. 201510616004). We greatly appreciate the support of the China Scholarship Council, and are thankful for the support of the Scientific Innovation Team of Remote Sensing Science and Technology of Chengdu University of Technology (Grant No. KYTD201501). The authors greatly appreciate Gabriela Shirkey for her editorial advice and comments. We are also grateful for the anonymous reviewer and his insight and critical review of the manuscript. Lastly, Huaiyong Shao, the author is grateful to the Center for Global Change and Earth Observations of Michigan State University for their workspace.

## Compliance with Ethical Standards

**Conflict of interest** The authors declare that they have no conflict of interest.

## References

- Aba County People's Government, P.R.China. (2012). The basic situation of Aba. [http://www.abaxian.gov.cn/xqgk/jbxq/201506/t20150612\\_1073279.html](http://www.abaxian.gov.cn/xqgk/jbxq/201506/t20150612_1073279.html). Accessed on December 16, 2015.
- Akiyama, T., & Kawamura, K. (2007). Grassland degradation in China: Methods of monitoring, management and restoration. *Grassland Science*, 53(1), 1–17. doi:10.1111/j.1744-697X.2007.00073.x.
- Asner, G. P., Borghi, C. E., & Ojeda, R. A. (2003). Desertification in central Argentina: Changes in ecosystem carbon and nitrogen from imaging spectroscopy. *Ecological Applications*, 13(3),

- 629–648. [https://doi.org/10.1890/1051-0761\(2003\)013\[0629:DICACI\]2.0.CO;2](https://doi.org/10.1890/1051-0761(2003)013[0629:DICACI]2.0.CO;2).
- Beyene, S. (2013). Rangeland degradation in a semi-arid communal savannah of Swaziland: Long-term dip-tank use effects on woody plant structure, cover and their indigenous use in three soil types. *Land Degradation and Development*, 26(4), 311–323. doi:10.1002/ldr.2203.
- Brandt, J. S., & Townsend, P. A. (2006). Land use–land cover conversion, regeneration and degradation in the high elevation Bolivian Andes. *Landscape Ecology*, 21(4), 607–623. doi:10.1007/s10980-005-4120-z.
- Cai, D., Guan, Y., Guo, S., Zhang, C., & Fraedrich, K. (2014). Mapping plant functional types over broad mountainous regions: A hierarchical soft time-space classification applied to the Tibetan Plateau. *Remote Sensing*, 6(4), 3511–3532. doi:10.3390/rs6043511.
- Cai, H., Yang, X., & Xu, X. (2015). Human-induced grassland degradation/restoration in the central Tibetan Plateau: The effects of ecological protection and restoration projects. *Ecological Engineering*, 83(83), 112–119. doi:10.1016/j.ecoleng.2015.06.031.
- Chaudhry, F., Wu, C. C., & Liu, W. (2006). Pixel purity index-based algorithms for endmember extraction from hyperspectral imagery. *Recent Advances in Hyperspectral Signal and Image Processing*, 661(2), 29–62.
- Chen, B. X., Tao, J., Wu, J. S., Wang, J. S., Zhang, J. L., Shi, P. L., et al. (2013). Causes and restoration of degraded alpine grassland in northern Tiber. *Journal of Resources and Ecology*, 4(1), 43–49. doi:10.5814/j.issn.1674-764x.2013.01.006.
- Chien, W. H., Wang, T. S., Yeh, H. C., & Hsieh, T. K. (2016). Study of NDVI application on turbidity in reservoirs. *Journal of the Indian Society of Remote Sensing*, 44(5), 1–8. doi:10.1007/s12524-015-0533-6.
- Collado, A. D., Chuvieco, E., & Camarasa, A. (2002). Satellite remote sensing analysis to monitor desertification processes in the crop-rangeland boundary of Argentina. *Journal of Arid Environments*, 52(1), 121–133. doi:10.1006/jare.2001.0980.
- Dawelbait, M., & Morari, F. (2012). Monitoring desertification in a savannah region in Sudan using landsat images and spectral mixture analysis. *Journal of Arid Environments*, 80(80), 45–55. doi:10.1016/j.jaridenv.2011.12.011.
- Dennison, P. E., & Roberts, D. A. (2003). Endmember selection for multiple endmember spectral mixture analysis using endmember average RMSE. *Remote Sensing of Environment*, 87(2–3), 123–135. doi:10.1016/S0034-4257(03)00135-4.
- Dong, Q. M., Zhao, X. Q., Wu, G. L., & Chang, X. F. (2015). Optimization yak grazing stocking rate in an alpine grassland of Qinghai-Tibetan Plateau, China. *Environmental Earth Sciences*, 73(5), 2497–2503. doi:10.1007/s12665-014-3597-7.
- Elmore, A. J., Mustard, J. F., Manning, S. J., & Lobell, D. B. (2000). Quantifying vegetation change in semiarid environments: Precision and accuracy of spectral mixture analysis and the normalized difference vegetation index. *Remote Sensing of Environment*, 73(1), 87–102. doi:10.1016/S0034-4257(00)00100-0.
- Fan, J. W., Zhong, H. P., Chen, H., Li, B., & Zhang, W. Y. (2007). Some scientific problems of grassland degradation in arid and semi-arid regions in northern China. *Chinese Journal of Grassland*, 29(5), 95–101. (in Chinese).
- Gao, Q. Z., Wan, Y. F., Xu, H. M., Li, Y., Wangzha, J. C., & Borjigidai, A. (2010). Alpine grassland degradation index and its response to recent climate variability in northern Tibet, China. *Quaternary International*, 226(1), 143–150. doi:10.1016/j.quaint.2009.10.035.
- Geerken, R., & Ilaiwi, M. (2004). Assessment of rangeland degradation and development of a strategy for rehabilitation. *Remote*

- Sensing of Environment*, 90(4), 490–504. doi:10.1016/j.rse.2004.01.015.
- Ghatol, S. G., & Karale, R. L. (2000). Assessment of degraded lands of Vidarbha region using remotely sensed data. *Journal of the Indian Society of Remote Sensing*, 28(2–3), 213–219. doi:10.1007/BF02989905.
- Green, A. A., Berman, M., Switzer, P., & Craig, M. D. (1988). A transformation for ordering multispectral data in terms of image quality with implications for noise removal. *IEEE Transactions on Geoscience and Remote Sensing*, 26(1), 65–74. doi:10.1109/36.3001.
- Harris, R. B. (2009). Rangeland degradation on the Qinghai-Tibetan Plateau: A review of the evidence of its magnitude and causes. *Journal of Arid Environments*, 74(1), 1–12. doi:10.1016/j.jaridenv.2009.06.014.
- Huang, S., & Siegert, F. (2006). Land cover classification optimized to detect areas at risk of desertification in North China based on spot vegetation imagery. *Journal of Arid Environments*, 67(2), 308–327. doi:10.1016/j.jaridenv.2006.02.016.
- Jenks, G. F. (1967). The data model concept in statistical mapping. *International Yearbook of Cartography*, 7, 186–190.
- Krishan, G., Kushwaha, S. P. S., & Velmurugan, A. (2009). Land degradation mapping in the upper catchment of river tons. *Journal of the Indian Society of Remote Sensing*, 37(1), 119–128. doi:10.1007/s12524-009-0003-0.
- Kuzera, K., Rogan, J., & Eastman, R. (2005). Monitoring vegetation re-growing and deforestation using change vector analysis: Mt. St. Helens study area. In *ASPRS 2005 Annual Conference Baltimore, MD*.
- Li, Q-F, & Du, W-H. (2013) Effect of the different width of ridge-furrow planting on corn growth in semi-arid areas of Longdong. *Grassland and Turf*.
- Li, H., Cai, Y. L., Chen, R. S., Chen, Q., & Yan, X. (2011). Effect assessment of the project of grain for green in the karst region in southwestern china: A case study of Bijie Prefecture. *Acta Ecologica Sinica*, 31(12), 3255–3264. (in Chinese).
- Li, X. L., Gao, J., Brierley, G., Qiao, Y. M., Zhang, J., & Yang, Y. W. (2013a). Rangeland degradation on the Qinghai-Tibet Plateau: Implications for rehabilitation. *Land Degradation and Development*, 24(1), 72–80. doi:10.1002/ldr.1108.
- Li, X. L., Perry, L. W. G., Brierley, G., Gao, J., Zhang, J., & Yang, Y. W. (2013b). Restoration prospects for Heitutan degraded grassland in the Sanjiangyuan. *Journal of Mountain Science*, 10(4), 687–698. doi:10.1007/s11629-013-2557-0.
- Li, Z. G., Han, G. D., Zhao, M. L., Wang, J., Wang, Z. W., & Kemp, D. R. (2015). Identifying management strategies to improve sustainability and household income for herders on the desert steppe in inner Mongolia, China. *Agricultural Systems*, 132, 62–72. doi:10.1016/j.agry.2014.08.011.
- Liu, M., Dries, L., Heijman, W., Huang, J., Zhu, X., Hu, Y. N., et al. (2017). *The impact of ecological construction programs on grassland conservation in inner Mongolia*. China: Land Degradation & Development. doi:10.1002/ldr.2692.
- Lorena, R. B., Santos, J. R., Shimabukuro, Y. E., Brown, I. F., & Kux, H. J. H. (2002). A change vector analysis technique to monitor land use/land cover in sw Brazilian Amazon: Acre state. *ECORA 15-Integrating Remote Sensing at the Global, Regional and Local Scale*, 8-15.
- Lu, D., Batistella, M., Moran, E., & Mausel, P. (2004). Application of spectral mixture analysis to Amazonian land-use and land-cover classification. *International Journal of Remote Sensing*, 25(23), 5345–5358. doi:10.1080/01431160412331269733.
- McMaster, R., & McMaster, S. (2002). A history of twentieth-century American academic cartography. *Cartography and Geographic Information Science*, 29(3), 312–315. doi:10.1559/152304002782008486.
- Mukherjee, S., Shashtri, S., Singh, C. K., Srivastava, P. K., & Gupta, M. (2009). Effect of canal on land use/land cover using remote sensing and GIS. *Journal of the Indian Society of Remote Sensing*, 37(3), 527–537. doi:10.1007/s12524-009-0042-6.
- Myint, S. W., & Okin, G. S. (2009). Modelling land-cover types using multiple endmember spectral mixture analysis in a desert city. *International Journal of Remote Sensing*, 30(9), 2237–2257. doi:10.1080/01431160802549328.
- Nackaerts, K., Vaesen, K., Muys, B., & Coppin, P. (2005). Comparative performance of a modified change vector analysis in forest change detection. *International Journal of Remote Sensing*, 26(5), 839–852. doi:10.1080/0143116032000160462.
- Niu, T. L., Liu, X. H., Zhou-Yuan, L. I., Gao, Y. Y., Kejia, D. E., & Wang, X. (2013). The spatio-temporal changes of the grassland in Ma county, the source region of the Yellow river during 1990–2009. *Environmental Science and Technology*, 36, 438–442. (in Chinese).
- Okin, G. S., & Roberts, D. A. (2004). Remote sensing in arid environments: Challenges and opportunities. In S. L. Ustin (Ed.), *Remote sensing for natural resource management and environmental monitoring* (pp. 11–146). New York: Wiley.
- Peddle, D. R., Hall, F. G., & Ledrew, E. F. (1999). Spectral mixture analysis and geometric-optical reflectance modeling of boreal forest biophysical structure. *Remote Sensing of Environment*, 67(67), 288–297. doi:10.1016/S0034-4257(98)00090-X.
- Powell, R. L., Roberts, D. A., Dennison, P. E., & Hess, L. L. (2007). Sub-pixel mapping of urban land cover using multiple endmember spectral mixture analysis: Manaus, Brazil. *Remote Sensing of Environment*, 106(2), 253–267. doi:10.1016/j.rse.2006.09.005.
- Ren, J. Z. (1998). *Grassland scientific research methods*. Beijing: China Agricultural Publishing House. (in Chinese).
- Röder, A., Udelhoven, T. H., Hill, J., Barrio, G., & Tsiourlis, G. (2008). Trend analysis of Landsat-TM and -ETM + imagery to monitor grazing impact in a rangeland ecosystem in Northern Greece. *Remote Sensing Environment*, 112, 2863–2875. doi:10.1016/j.rse.2008.01.018.
- Shao, H. Y., Liu, M., Shao, Q. F., Sun, X. F., Wu, J. H., & Xiang, Z. Y. (2014). Research on eco-environmental vulnerability evaluation of the Anning River Basin in the upper reaches of the Yangtze River. *Environmental Earth Sciences*, 72(5), 1555–1568. doi:10.1007/s12665-014-3060-9.
- Shao, H. Y., Sun, X. F., Wang, H. X., Zhang, X. X., Xiang, Z. Y., & Tan, R. (2016). A method to the impact assessment of the returning grazing land to grassland project on regional eco-environmental vulnerability. *Environmental Impact Assessment Review*, 56, 155–167. doi:10.1016/j.ear.2015.10.006.
- Small, C. (2001). Estimation of urban vegetation abundance by spectral mixture analysis. *International Journal of Remote Sensing*, 22(7), 299–307. doi:10.1080/01431160151144369.
- The Animal Husbandry Bureau of Sichuan Province. Grassland monitoring report of Sichuan Province in 2012. <http://www.grassland.gov.cn/grassland-new/Item/4928.aspx>, 2013. Accessed on July 1, 2015.
- Wessels, K. J., Pretorius, D. J., & Prince, S. D. (2008). Reality of rangeland degradation mapping with remote sensing: The South African experience. In *14th Australasian remote sensing and photogrammetry conference, Darwin, Australia*.
- Wu, C. (2004). Normalized spectral mixture analysis for monitoring urban composition using ETM + imagery. *Remote Sensing of Environment*, 93(4), 480–492. doi:10.1016/j.rse.2004.08.003.
- Wu, C., & Murray, A. (2003). Estimating impervious surface distribution by spectral mixture analysis. *Remote Sensing of Environment*, 84(4), 493–505. doi:10.1016/S0034-4257(02)00136-0.
- Yang, A. X., Yang, T., Ji, Q., He, Y., & Ghebregabher, M. G. (2014). Regional-scale grassland classification using moderate-

- resolution imaging spectrometer datasets based on multistep unsupervised classification and indices suitability analysis. *Journal of Applied Remote Sensing*, 8, 1261–1264. doi:[10.1117/1.JRS.8.083548](https://doi.org/10.1117/1.JRS.8.083548).
- Zhang, J. T. (2006). Grassland degradation and our strategies: A case from Shanxi province, China. *Rangelands*, 28(1), 37–43. [https://doi.org/10.2111/1551-501X\(2006\)28.1\[37:GDAOSA\]2.0.CO;2](https://doi.org/10.2111/1551-501X(2006)28.1[37:GDAOSA]2.0.CO;2).
- Zhang, Z. B., Ke, C. Q., & Shang, Y. J. (2014). Studying changes in land use within the Poyang lake region. *Journal of the Indian Society of Remote Sensing*, 42(3), 633–643. doi:[10.1007/s12524-013-0348-2](https://doi.org/10.1007/s12524-013-0348-2).
- Zhao, J., Luo, T., Li, R., Li, X., & Tian, L. (2016) Grazing effect on growing season ecosystem respiration and its temperature sensitivity in alpine grasslands along a large altitudinal gradient on the central Tibetan Plateau. *Agricultural and Forest Meteorology*, 218–219, 114–121. <https://doi.org/10.1016/j.agrformet.2015.12.005>.